New Hexafunctional Epoxy Prepolymer: Innovation structure in corrosion inhibition

Naoual El-Aouni
University Ibn Tofail
Omar Dagdag
omar.dagdag@uit.ac.ma
Gachon University
Abdeslam EL AMRI
Ibn Tofail University
Hansang Kim
Gachon University
Nadia Dkhireche
Ibn Tofail University
Abderrahim Elbachiri
Boulevard Sour-Jdid
Elyor Berdimurodov
New Uzbekistan University
Avni Berisha
University of Prishtina
Mohamed Rafik
University Ibn Tofail
Nizomiddin Aliev
Tashkent State University of Economics

Research Article

Keywords: Epoxy prepolymer, HGTMDAP, metal corrosion, surface characterization and electrochemistry

Posted Date: January 24th, 2024

DOI: https://doi.org/10.21203/rs.3.rs-3869534/v1

Additional Declarations: No competing interests reported.

Version of Record: A version of this preprint was published at Journal of Bio- and Tribo-Corrosion on April 24th, 2024. See the published version at https://doi.org/10.1007/s40735-024-00844-2.

New Hexafunctional Epoxy Prepolymer: Innovation structure in corrosion inhibition

Naoual El-Aouni[1], Omar Dagdag[2]*, Abdeslam EL AMRI[3], Hansang Kim[2]*, Nadia Dkhireche[3], Abderrahim Elbachiri[4], Elyor Berdimurodov[5,6,7]*, Avni Berisha[8] and Mohamed Rafik[1] and Nizomiddin Aliev[9]

[1]Laboratory of Organic Chemistry, Catalysis and Environment, Department of Chemistry, Faculty of Sciences, University Ibn Tofail, BP 242, 14000 Kenitra, Morocco

[2]Department of Mechanical Engineering, Gachon University, Seongnam 13120, Republic of Korea

[3]Laboratory of Advanced Materials and Process Engineering, Faculty of Sciences, Ibn Tofail University, BP 242, Kenitra, 14000, Morocco

[4]Royal Naval School, University Department –Boulevard Sour-Jdid, Casablanca, Morocco

[5]Chemical & Materials Engineering, New Uzbekistan University, 54 Mustaqillik Ave., Tashkent 100007, Uzbekistan

[6]Medical School, Central Asian University, Tashkent 111221, Uzbekistan

[7]Faculty of Chemistry, National University of Uzbekistan, Tashkent 100034, Uzbekistan

[8]Department of Chemistry, Faculty of Natural and Mathematics Science, University of Prishtina, 10000 Prishtina, Albania.

[9]Tashkent State University of Economics, Tashkent, 100066 Uzbekistan

Corresponding authors E-mail: omar.dagdag@uit.ac.ma, hskim70@gachon.ac.kr, elyor170690@gmail.com

Abstract

This work presents a novel approach to corrosion inhibition through the creation of a groundbreaking hexafunctional phosphorus epoxy resin, namely phosphorus trimethylene dianiline hexaglycidyl (HGTMDAP). This innovative material is synthesized via a two-step process, initiating with a grafting reaction between methylene dianiline and phosphorus trichloride, followed by the addition of epichlorohydrin to yield the hexafunctional resin. The unique structural intricacies of this material were elucidated using advanced microscopic characterization techniques such as FTIR, ^{1}H, and ^{13}C NMR. Furthermore, we dove into the exploration of the anticorrosive efficacy of this novel epoxy resin, specifically for metal, leveraging an array of evaluation methods, including EIS, PDP, isothermal adsorption model, thermodynamics, EFM, and the cutting-edge DFT, MC and MD simulations. To explore surface adsorption mechanism of the medium, comprising the metallic material, HGTMDAP resin, and 1.0 M HCl, it was employed sophisticated techniques such as SEM and EDS. This enabled us to decode the surface structure and chemical composition of the sample, providing us with a deeper understanding of the adsorption process and the mechanics of corrosion prevention. Our findings from the electrochemical tests suggest that an increase in the concentration of HGTMDAP significantly enhances protection ability. Interestingly, EIS demonstrated an impressive inhibition efficiency of 96.3% at the optimal concentration (10^{-3} M) of HGTMDAP epoxy resin. Polarization results further corroborated that this advanced macromolecular binder serves as a mixed inhibitor. The Langmuir model, which posits that the epoxy resin forms a defender film on the metal surface, was validated in our study. We also utilized kinetic thermodynamic parameter estimation to further evaluate inhibitor adsorption phenomena. Finally, it was ventured into unchartered territory by describing the electronic and adsorption properties of the HGTMDAP epoxy resin using DFT, MC and MD simulations, paving the way

for future research in this domain. Through our innovative approach, we have opened up new possibilities in the field of corrosion inhibition.

Keywords: Epoxy prepolymer, HGTMDAP, metal corrosion, surface characterization and electrochemistry.

1. Introduction

When a metal corrodes, it means that it has deteriorated and degraded as a result of chemical or electrochemical reactions with its surroundings. It affects many businesses, including manufacturing, infrastructure, transportation, and energy generation, and it is expensive. Due to the cost of maintaining, replacing, and repairing rusted metal structures and equipment, corrosion can result in large economic losses. Corrosion-related direct costs include material replacement, labour, and repair downtime. Reduced production, environmental effects, and potential safety risks all have indirect costs [1]. Protective agent s are frequently used to lessen the damaging effects of corrosion and increase the lifespan of metal assets. Protective agent s are compounds that can either be applied directly to the metal surface or added to the corrosive environment to delay or reduce the corrosion process. They function by creating a layer of defence that serves as a barrier against corrosive substances on the metal surface. The usage of protective agent s has a number of benefits. First off, they can considerably slow down corrosion, extending the useful life of metal buildings and machinery. By reducing the need for regular repairs or replacements, this results in cost savings. Second, compared to other corrosion protection strategies like coatings or alloy selection, protective agent s may be more economical. They are frequently compatible with current systems, easy to implement, and low maintenance [2-4]. The two primary groups of inhibitors are organic and inorganic inhibitors. On chemical substances and salts, inorganic inhibitors like chromates, phosphates, and silicates are based. Through the creation of a passivating layer on the metal surface, they offer corrosion protection. However, because of their toxicity and contamination potential, the usage of several inorganic inhibitors has sparked environmental concerns [5-7]. On the other hand, organic inhibitors are generated from organic substances and are typically less harmful to humans and the environment. They frequently contain functional groups that can interact chemically with the metal surface and form a shield, including amines, carboxylates, or phosphates. Organic inhibitors are adaptable to particular applications and have good material compatibility [8]. The kind of metal, the corrosive environment, the temperature, and the required lifespan of protection all play a role in choosing an appropriate protective agent . Protective agent s are put through rigorous testing and research to see how well they operate in particular applications [9, 10]. Metal corrosion is a costly problem that affects various industries. The use of protective agent s provides an effective and economical solution to protect metals from corrosion. By applying inhibitors, the rate of corrosion can be reduced, leading to cost savings, extended asset lifespan, and improved operational efficiency. The choice of protective agent depends on the specific application requirements and environmental considerations [8]. In the field of protective agent s, organic macromolecules show great potential and are preferred over inorganic inhibitors due to concerns about their ecotoxicity. Organic inhibitors are typically derived from by-products of the petroleum industry or synthesized compounds [11, 12]. Carbon steel, being cost-effective, is increasingly utilized in various industries. Hydrochloric acid finds frequent use in industrial processes for cleaning and pickling. However, due to the aggressive

nature of this acidic solution, the use of protective agent s is necessary to reduce the rate of metal corrosion [13].

The main aim of this research is to develop a new hexafunctional phosphorus epoxy resin, HGTMDAP, and evaluate its effectiveness as a protective agent for metal. The research involves synthesizing the resin through a two-step process and characterizing its structural properties using advanced microscopic techniques. Various evaluation methods, including EIS, PDP, isothermal adsorption model, temperature effect, thermodynamic parameters, EFM, and SEM/EDS analysis, are used to understand the inhibition mechanism and surface adsorption. The findings demonstrate the enhanced protection ability of the HGTMDAP resin and validate its potential as a protective agent . Additionally, DFT, MC, and MD simulations are employed to describe the electronic and adsorption properties of the resin. This research opens up new possibilities for corrosion inhibition strategies.

2. Experimental materials and methods

2.1. Materials used

The products used are phosphorus trichloride, methylene dianiline (MDA), methanol and epichlorohydrin which is kept at 99 % purity stored at about 4-6°C. All these base products were supplied by Acros Chemical Company and Aldrich Chemical Company, with no further purification.

2.2. Synthesis of hexaglycidyl trimethylene dianiline phosphorus (HGTMDAP).

The two-step synthesis of a new phosphorus trimethylene dianiline hexaglycidyl epoxy resin (HGTMDAP) will be presented in this study according to the following reaction scheme (**Figure 1**).

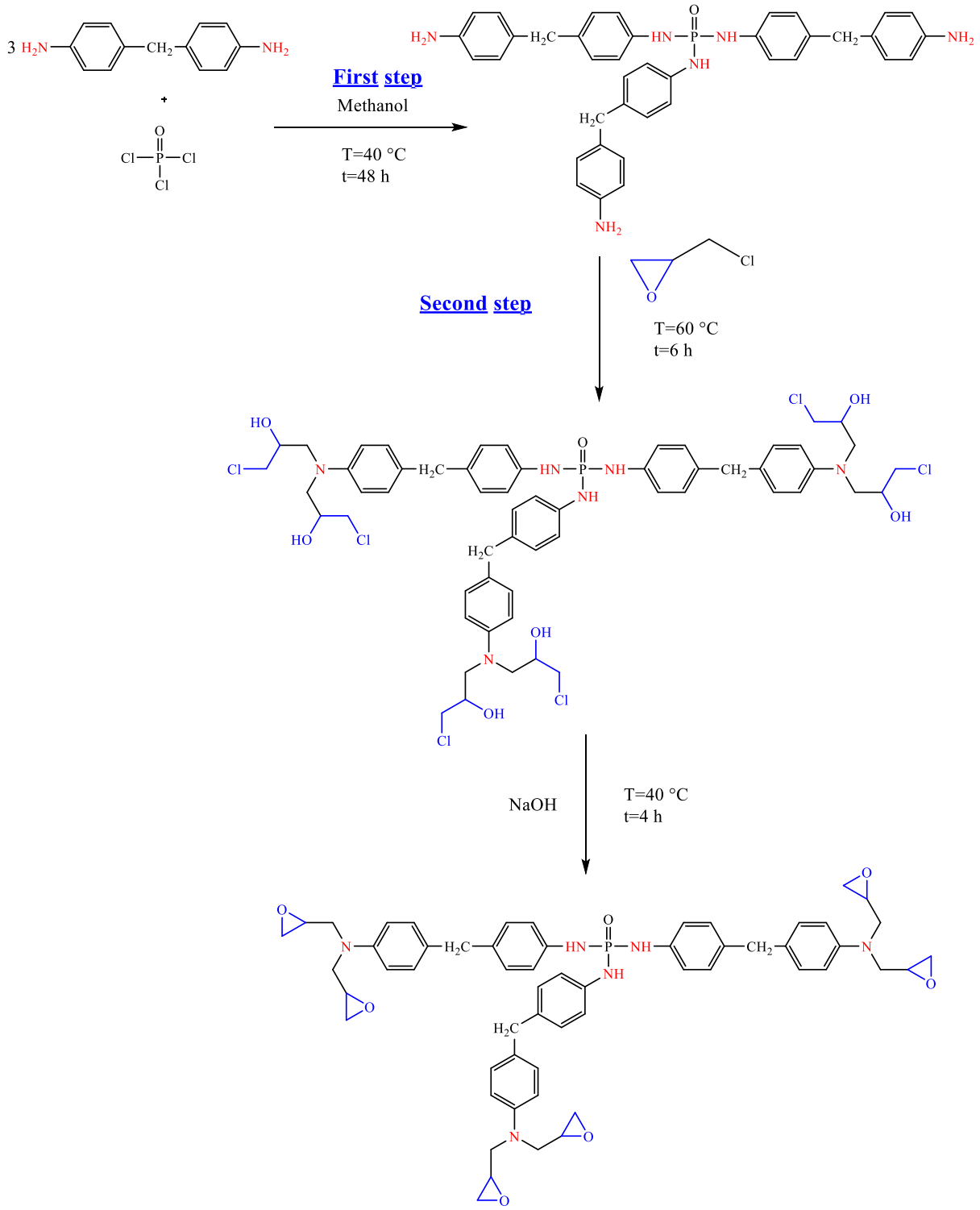

Figure 1: Schematic diagram for the synthesis of hexaglycidyl trimethylene dianiline phosphorus (HGTMDAP).

2.2.1. Experimental protocol for the synthesis of the new phosphorus trimethylene dianiline hexaglycidyl epoxy resin (HGTMDAP).

The synthesis of hexaglycidyl trimethylene dianiline phosphorus resin (HGTMDAP), a new resin, is carried out in two reaction steps. Initially, $3.9.10^{-2}$ mol methylene dianiline dissolved in 50 ml methanol and $13.04.10^{-3}$ mol phosphorus trichloride are mixed. The mixture must be kept at 40°C and shaken vigorously for 48 hours. Next, 7.8x10-2 mol of

epichlorohydrin is added. The mixture is heated to 80 °C and magnetically stirred constantly for a whole day. A later step. After cooling to 40 °C, $7.82*10^{-2}$ mol of a solution containing NaOH at the rate of one half its weight by mass is added into water and left agitating for an hour and twenty minutes (50 min.). Next, water is added to the organic phase. Finally chloroform is used to eliminate it. Using a rotary evaporator, anhydrous sodium sulphate (Mg_2SO_4) is dried and the solvent is removed. In 89% of cases, a viscous resin product is produced.

2.3. Structural analysis methods

2.3.1. FTIR

A BRUKER FTIR infrared spectrometer was employed. Bands on Attenuated Total Reflectance (ATR) were obtained during transmission. Between 2.5 and 25 µm is the spectral range that corresponds to the vibrational energy of the molecules. In the range of 500 cm^{-1} to 7000 cm^{-1}, analysis was done.

2.3.2. NMR

The product was dissolved in DMSO to conduct ^{1}H and ^{13}C NMR studies using a BRUKER AVANCE 300MHz equipment. The unit of chemical shift is ppm.

2.4. Metal and corrosive solution

A of E24 carbon steel, which has a material surface area of 1 cm^2. The residual material is mostly iron (Fe). The system under study was a 1.0 M HCl. This was done by diluting a commercial 37 % HCl solution with distilled water. The concentrations of inhibitors vary from 10^{-6} to 10^{-3} M. This concentration range was established by examining the HGTMDAP inhibitor prepolymer's solubility in a corrosive solution.

2.5. Electrochemical measurement

A three-electrode electrochemical cell has been assembled for electrochemical measurements. It is made up of a platinum counter electrode, a saturated calomel reference electrode, and a metal working electrode. PDP was done with a Gamry PCI4-G750 Potentiostat/Galvanostat/Zra. First, the working electrode was submerged in the free corrosion potential for 20 minutes. It can scan at a rate of 0.5 mV/s. To compute the electrochemical parameters, utilise the Gamry Framework - Gamry Echem Analyst programme. Consequently, inhibitory efficacy is determined using Equation 1.

$$\mathrm{IE}(\%) = \left(\frac{i_{\mathrm{corr}}^{0} - i_{\mathrm{corr}}}{i_{\mathrm{corr}}^{0}} \right) \times 100 \qquad (1)$$

Transient electrochemical measurements at a signal amplitude of 10 mV were assessed using the same apparatus. The range of frequencies covered by the study is 100 KHz–10 mHz. To compute the inhibitory efficiency, use Equation 2.

$$\mathrm{IE}\% = \left(\frac{R_{\mathrm{ct}} - R_{\mathrm{ct}}^{0}}{R_{\mathrm{ct}}} \right) \times 100 \qquad (2)$$

2.6. SEM-EDX

The research procedures for SEM-EDX analysis in studying protective agent s typically involve the following steps:

Sample Preparation: Prepare the metal samples by cleaning them thoroughly to remove any contaminants or surface oxides. This can be done using appropriate cleaning methods such

as solvent cleaning, ultrasonic cleaning, or mechanical polishing. Ensure that the samples are properly dried before proceeding to the next step.

SEM Imaging: Place the coated samples in the SEM chamber and adjust the instrument settings for imaging. Choose appropriate magnification and operating parameters such as accelerating voltage and beam current based on the sample and desired resolution. Capture SEM images of the sample surface to examine its morphology and topography.

EDX Analysis: Perform EDX analysis to research the elemental composition of the sample. Select specific regions of interest on the SEM images for EDX analysis, such as the metal surface or the interface between the metal and the protective agent . Acquire EDX spectra from these regions to obtain information about the chemical elements present and their relative concentrations.

2.7. Theoretical investigations

The research methodology for theoretical investigations in this study involves the use of DFT calculations and molecular simulations (MC and MD) to study the interactions between the HGTMDAP inhibitor and the metal interface. The specific details of the methodology are as follows [14, 15]:

1. DFT Calculations:
   - ✓ Dmol3 Module: DFT calculations are approved by the Dmol3 module that is built into the Biovia Materials Studio programme [16-18].
   - ✓ Geometry Optimization: Generalized Gradient Approximation (GGA) employing the pbe functional is used for geometry optimizations of the molecular structures [19].
   - ✓ Numerical Basis Set: A double-sized numerical basis set plus d-functional (DND) is utilized for the calculations.

1. MC and MD Simulations [1, 5, 20-23]:
   - ✓ Purpose: The MC and MD simulations are conducted to study and understand the interactions between the protonated and neutral HGTMDAP forms and the metal interface.
   - ✓ Simulation Software: Materials Studio 8.0 software is employed for performing the MC and MD simulations.
   - ✓ Methodology: The simulations entail identifying various adsorption configurations and examining the system of interactions between the metal and the HGTMDAP inhibitor's molecular structure.

By employing these theoretical investigations, including DFT estimations and molecular simulations, the study aims to gain insights into the interactions between the HGTMDAP inhibitor and the metal interface, providing valuable information about the inhibitive properties and behavior of the inhibitor under different conditions.

3. Results and discussion

3.1. Spectral characterization of synthesized epoxy resin

Nucleophilic substitution of the aromatic NH_2 ambident rings of methylene dianiline by the chlorine of phosphorus trichloride $P(O)Cl_3$ and the chlorine of epichlorohydrin yields hexafunctionalized aromatic glycidylamines. FTIR and ^{1}H, ^{13}C NMR spectroscopy have proven and demonstrated this.

3.1.1. FTIR structural study

The given IR spectrum bands for the phosphorus trimethylene dianiline hexaglycidyl (HGTMDAP) provide important information about its functional groups and chemical bonds (**Figure SI1 and Table SI1**):

3691.84 cm^{-1} (Band: ν OH): This peak is equivalent to the stretching vibration of hydroxyl (OH) groups. OH groups indicate hydroxyl functional groups in the molecule.

3300.67 cm^{-1} (Band: Elongation of the secondary amine group (-NH-): This peak corresponds to the elongation (stretching) vibration of secondary amine groups (-NH). The presence of secondary amine functional groups in the molecule is implied.

2837.45 cm^{-1} (Band: Aliphatic methylene ($-CH_2$)): This peak is the stretching vibration of aliphatic methylene ($-CH_2$) groups. It shows that there are methylene groups in the aliphatic part of the molecule.

1611.96 cm^{-1}, 1509.96 cm^{-1}, 1430.71 cm^{-1} (Bands: valence vibrations ($\nu C_{ar}=C_{ar}$)): The peaks are related to the valence vibrations of carbon-carbon (C=C) double bonds in aromatic rings. These vibrations are a typical indicator of the aromatic rings in the molecule.

1319.47 cm^{-1} (Band: Aromatic bond (C-N)): This peak is representative of the vibrations within carbon-nitrogen (C-N) bonds. It points to the existence of aromatic rings with nitrogen atoms in the molecule.

1045.46 cm^{-1} (Band: P(O)-N): This peak corresponds to a stretching vibration of the phosphorus-oxygen-nitrogen (P(O)-N) bonds. Such bonds are present in the molecule.

809.14 cm^{-1} (Band: Epoxy group): This peak is typical of the vibration of epoxy (oxirane) groups. It implies an epoxy functional group in the molecule.

751.09 cm^{-1} (Band: Vibration of the aromatic C-H bond): This peak corresponds to the vibration of the aromatic carbon-hydrogen (C-H) bonds. It confirms the presence of aromatic rings in the molecule.

3.1.2. ^{1}H and ^{13}C NMR characterization

With its data from the ^{13}C NMR (**Figure SI2**) and ^{1}H NMR (**Figure SI3**) spectra for HGTMDAP, we gain some valuable information about this compound's chemical environment and structural features.

^{1}H NMR Spectrum (**Table SI2**):

2.458 - 2.465 ppm (dd, 2H, CH_2 oxirane): This peak represents two hydrogen atoms (2H) in the methylene group (CH_2) of an oxirane (epoxy) functional group. The presence of oxirane groups is confirmed.

3.519 - 3.599 ppm (m, 1H, CH oxirane): This peak corresponds to a single hydrogen atom (1H) in a methine group (CH) of an oxirane functional group. It also confirms the presence of oxirane groups.

3.607 - 3.640 ppm (dd, N-CH_2): This peak represents a methylene group (CH_2) linked to nitrogen (N). It suggests the presence of a secondary amine group (-NH) in the molecule.

3.86 ppm (CH_2 aliphatic methylene): This peak corresponds to a methylene group (CH2) in the aliphatic portion of the molecule.

3.87 ppm (Aromatic C-NH): This peak represents a hydrogen atom (H) attached to a nitrogen atom (N) in an aromatic ring. It indicates the presence of an aromatic amine group.

6.55 - 7.27 ppm (s, 4H, aromatic): This set of peaks indicates the presence of four hydrogen atoms (4H) in an aromatic ring. The chemical shift range and singlet (s) pattern confirm the presence of aromatic rings in the molecule.

^{13}C NMR Spectrum (**Table SI3**):

39.503 - 40.507 ppm (CH_2 aliphatic): This range represents carbon atoms (CH2) in the aliphatic portion of the molecule.

46.890 ppm (s, CH2, oxirane): This peak corresponds to a carbon atom (CH_2) in the oxirane (epoxy) functional group.

48.340 - 53.600 ppm (s, CH oxirane): This range represents carbon atoms (CH) in the oxirane functional group.

68.679 - 70.407 ppm (CH_2 linked to nitrogen): This range represents carbon atoms (CH_2) linked to nitrogen (N), confirming the presence of secondary amine groups in the molecule.

112.814 ppm (s, CH aromatic): This peak corresponds to a carbon atom (CH) in an aromatic ring.

123.225 ppm (s, C aromatic tertiary): This peak represents a tertiary carbon atom (C) in an aromatic ring.

130.197 ppm (s, C nitrogen-bonded aromatic tertiary): This peak indicates a tertiary carbon atom (C) in an aromatic ring, specifically bonded to nitrogen (N).

3.2. Polarization curves

3.2.1. Influence of concentration in the corrosion inhibition

The following main points were found related to effect of concentration (**Table 1**):

- ✓ The polarization curves show that the addition of HGTMDAP inhibitor decreased the i_{corr} in the unprotected system. Lower i_{corr} indicates lower corrosion rate with the inhibitor [24, 25]..
- ✓ i_{corr} decreased with rising inhibitor values, suggesting better inhibition efficiency at higher concentrations [26, 27].
- ✓ With the addition of inhibitor, the values of β_a and β_c, which stand for the anodic and cathodic Tafel slopes, respectively, either reduced or remained unchanged. This suggests that HGTMDAP functions as an inhibitor of mixed types.
- ✓ The protection values (η_{PDP}) calculated from i_{corr} values rose with increasing HGTMDAP values, achieving a maximum of 96.9% at 10^{-3} M. This confirms the good protection ability of HGTMDAP.
- ✓ The corrosion potential (E_{corr}) was not significantly changed with the addition of inhibitor. This implies that HGTMDAP acts mainly by decreasing the corrosion velocity [28, 29]..

In summary, the results demonstrate that HGTMDAP is an effective mixed-type inhibitor, and higher concentrations provided better inhibition efficiency through decreased corrosion current densities.

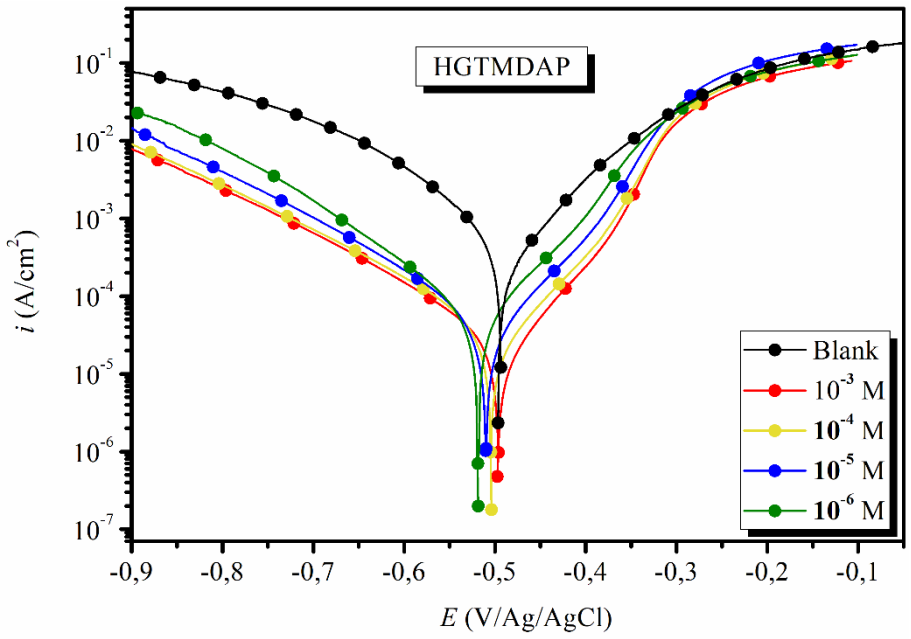

Figure 2: Tafel plots for blank and HGTMDAP.

Table 1. PDP characters for blank and HGTMDAP.

Compounds	Conc. (M)	- β_c (mV dec^{-1})	β_a (mV dec^{-1})	i_{corr} (µA cm^{-2})	E_{corr} (mV/Ag/AgCl)	η_{PDP} (%)
HCl 1.0 M	--	139	153	980	-497	------
HGTMDAP	10^{-3}	153	73.4	30	-492	96.9
	10^{-4}	161.8	78.9	43	-501	95.6
	10^{-5}	148.7	78.9	51	-505	94.8
	10^{-6}	139	90	83	-515	91.5

3.2.2. Effect of temperature

The basic comments from the effect of temperatures were follows (**Table 2**):

- ✓ The Tafel plots show that i_{corr} rises with growth temperature for the blank and inhibitor systems, showing that temperature has a detrimental influence on corrosion resistance.
- ✓ i_{corr} amounts were high protected system, demonstrating its good inhibition efficiency even at elevated temperatures [30, 31].
- ✓ The βc and βa values generally decrease with growing temperature for both systems. The decreased βa values with inhibitor suggest it acts by blocking the anodic active sites.
- ✓ E_{corr} shifts slightly towards negative potentials with increasing temperature but is not significantly influenced by the introduction of protection.

In summary, HGTMDAP exhibits efficient inhibition even at elevated temperatures up to 328K. While its performance decreases with temperature, it still provides good corrosion protection at higher temperatures through decreasing i_{corr} values.

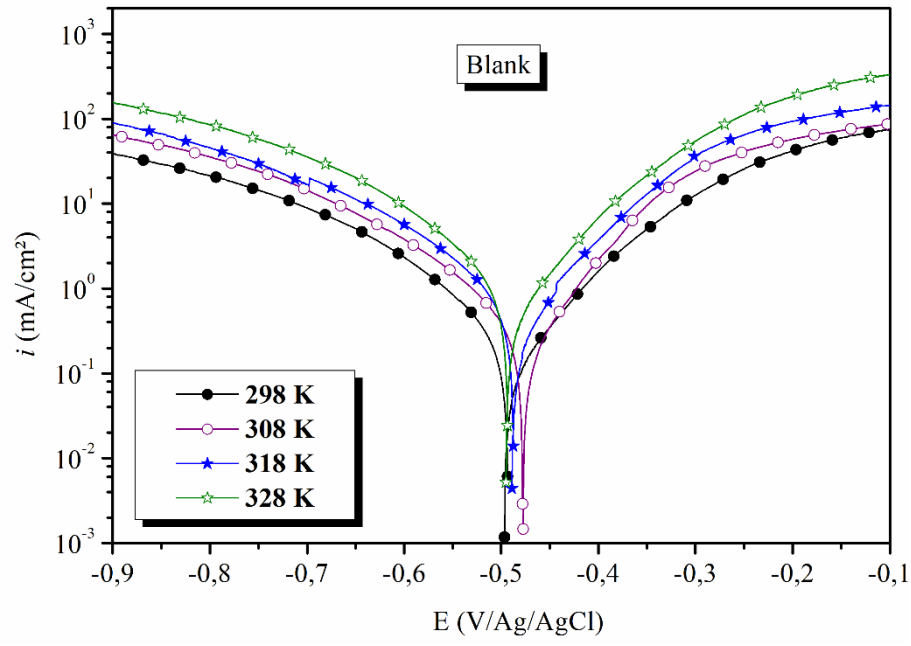

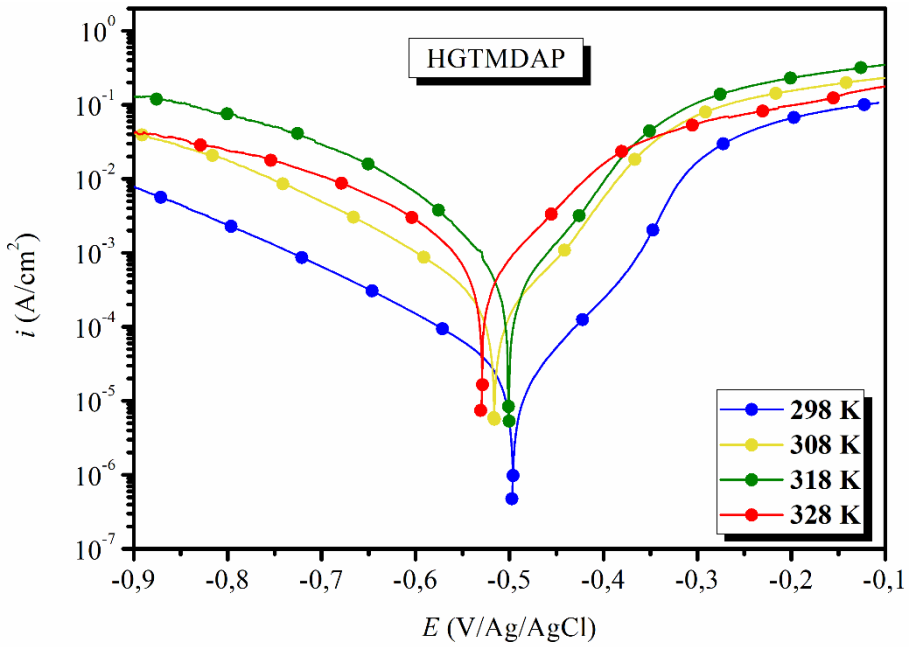

Figure 3: Tafel plots for blank and HGTMDAP (10^{-3} M) at various temperatures.

Table 2: PDP properties of blank and HGTMDAP (10^{-3} M) at different temperatures.

Compounds	T (K)	E_{corr} (mV/Ag/AgCl)	i_{corr} (μA cm^{-2})	$-\beta_c$ (mV.dec^{-1})	β_a (mV dec^{-1})
Blank	298	-497	980	139	153
	308	-491	1200	184	112
	318	-475	1450	171	124
	328	-465	2200	161	118
HGTMDAP	298	-492	30	153	73.4
	308	-512	94	65.8	66.7
	318	-496	182	47.5	62.5

	328	-525	335	72.5	78.8

3.2.3. Thermodynamic activation parameters

The temperature dependence of the corrosion velocity is indicated by the Arrhenius equation (**3**).

$$i_{corr} = k \exp\left(-\frac{E_a}{RT}\right) \qquad (3)$$

The ideal gas constant is R, and E_a is the activation energy. The pre-exponential factor is K, and the temperature is T. The Arrhenius equation and another version known as the transition state equation (4) were used to determine the thermodynamic properties of the corrosion reaction, such as E_a, S_a, and H_a:

$$i_{corr} = \frac{RT}{Nh} \exp\left(\frac{\Delta S_a}{R}\right) \exp\left(\frac{\Delta H_a}{RT}\right) \qquad (4)$$

Arrhenius diagrams for the temperature range 298 to 328 K are shown in **Figure 4**.

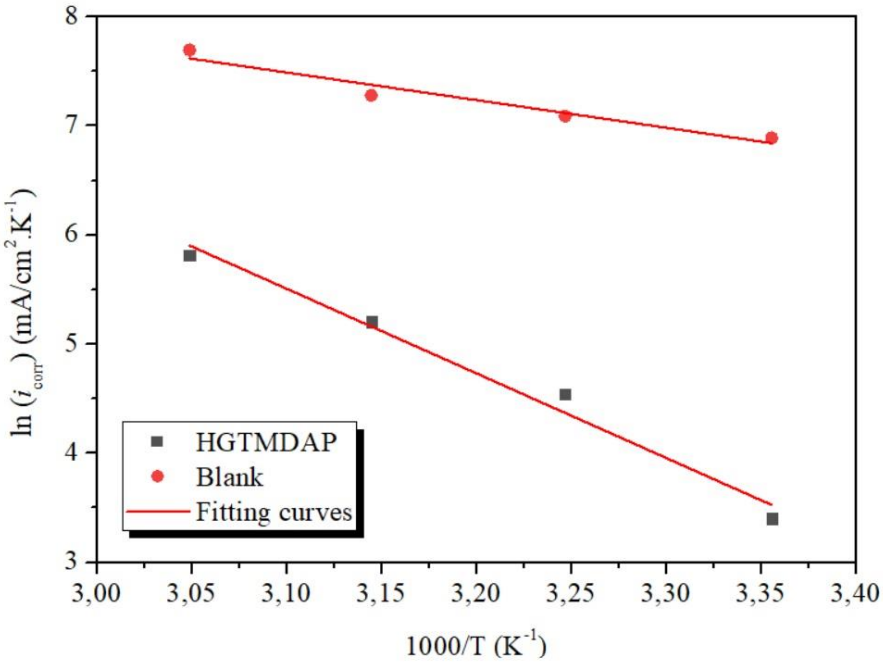

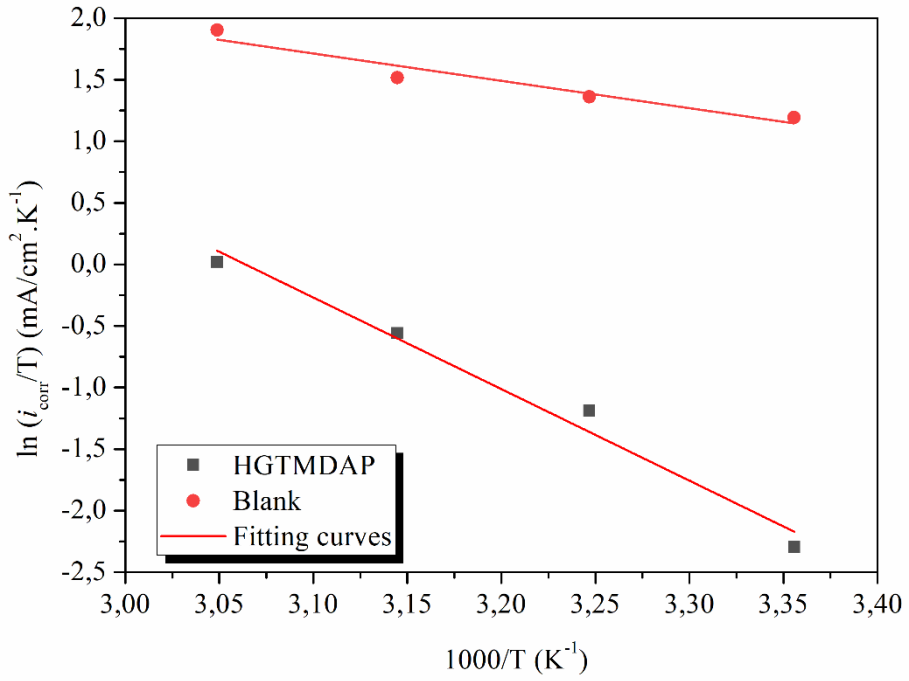

Figure 4: Arrhenius plots for 10^{-3} M HGTMDAP.

Table 3: Activation parameters for blank and 10^{-3} M HGTMDAP.

	E_a (kJ/mol)	ΔH_a (kJ/mol)	ΔS_a (J/mol.K)
Blank	23.29	18.71	-125.93
HGTMDAP	64.43	61.83	-8.08

Compared to the unprotected system, the inhibited solution has much greater values of E_a and ΔH_a (**Table 3**). This suggests that the inhibitor works as a barrier, making the corrosion process more challenging when present. These results show how apparent activation energy values change when an inhibitor is added. This suggests that adding an inhibitor to the solution reduces iron corrosion [32]. The endothermic dissolution of metal is confirmed by the positive indicate of ΔH_a (ΔH_a = 61.83 kJ/mol) of 1.0 M HCl [33].

The positive ΔH_a values endothermic nature of all chemical processes in the selected systems. The values of negative entropy (ΔS_a) suggest that an ordered layer of inhibitor molecules has formed on the metal surface, as the activated complex is less disordered in the transition state than the reactants. The strong, negative entropy value (ΔS_a = -8.08 J/mol.K) in 1.0M HCl indicates the formation of an activated complex during the velocity removal step, which limits the corrosion process. Moreover, the thermodynamic link between activation energy (E_a) and activation enthalpy (ΔH_a) is confirmed by the identical variations in variation of both as a function of HGTMDAP inhibitor concentration [34].

The higher thermodynamic activation parameters in the inhibited solution demonstrates that HGTMDAP functions by improving the energy blocks in all chemical dissolution of metal, thereby providing inhibition at elevated temperatures up to 328K.

3.3. EIS

The key points were found based on EIS results are:

- ✓ Nyquist plots show single capacitive loops becoming larger with increasing inhibitor concentration, indicating corrosion resistance increases [35, 36] (**Figure 5**).
- ✓ Bode plots show phase angle peaks shifting to higher frequencies with inhibitor, suggesting faster electrode kinetics [37, 38].
- ✓ Equivalent circuit fitting confirms single time constant system and introduction of good insulator of metal surface from the corrosion ions (**Figure 7**).
- ✓ R_{ct} values increase with HGTMDAP introduction, because, the active sites were effectively blocked with the HGTMDAP [38-40].
- ✓ θ and η_{EIS} values >95-96% even at lower concentrations indicate excellent inhibition efficiency of HGTMDAP confirmed by EIS (**Table 4**).
- ✓ Low Q and n values close to 1 demonstrate near ideal capacitive behavior of protective film.
- ✓ Good correlation between EIS and weight loss results.
- ✓ The expansion of the single capacitive loop diameter with rise the inhibitor values reflects a rise in thickness and protective quality of the HGTMDAP film on the metal surface.
- ✓ The shifts of the phase angle peak to higher frequencies indicate that HGTMDAP adsorb on the metal and block the corrosion sites, making the oxidation and reduction reactions slower.
- ✓ The near unity values of n close to 1 confirmed that the inhibitor film has a close to ideal capacitive behavior. This homogeneous and compact protective film inhibits corrosion.
- ✓ The decreasing Q values with increasing concentration reflect diminishing inhomogeneities of the inhibitor film. This correlates with better inhibition efficiency at higher concentrations.
- ✓ The excellent agreement between impedance data and equivalent circuit fitting validates the chosen circuit model and mechanism of inhibitor adsorption and film formation.
- ✓ Comparing EIS and polarization results, the similarities in trends of Rct, θ and icorr values with inhibitor concentration strongly support the proposed inhibition mechanism (**Figure 6**).
- ✓ The EIS results thus provide microscopic level insights into the adsorption and inhibition processes that cannot be obtained from weight loss or polarization techniques alone.

In summary, EIS reveals HGTMDAP functions by introduction barrier film on metal surface via adsorption, shifting kinetics to diffusion control and protecting steel even at low concentrations, as suggested by increased R_{ct}, θ and impedance values with concentration. Results confirm HGTMDAP as an effective inhibitor.

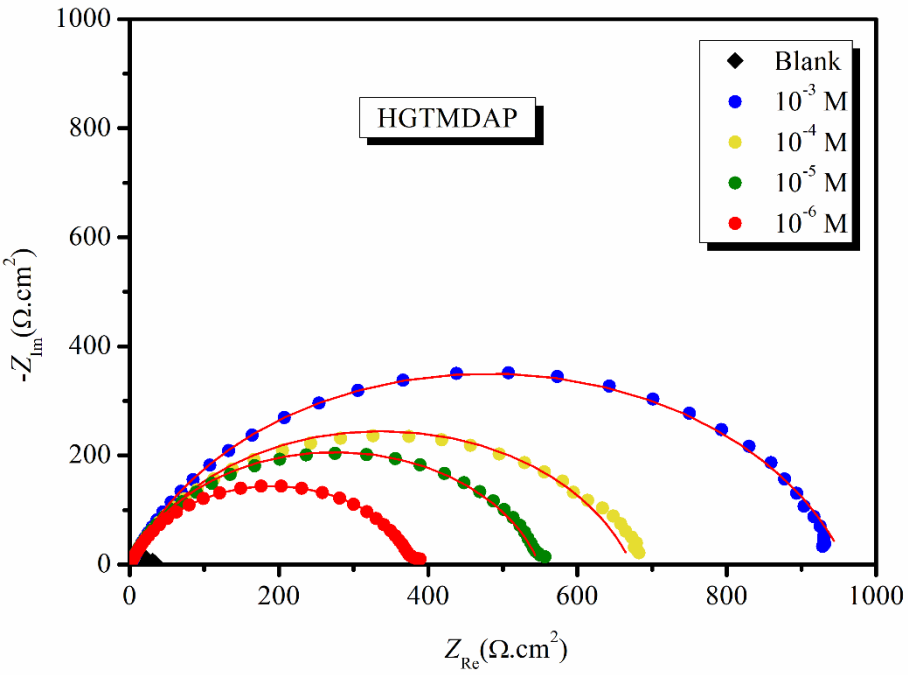

Figure 5: Nyquist plots for blank and HGTMDAP at 298 K.

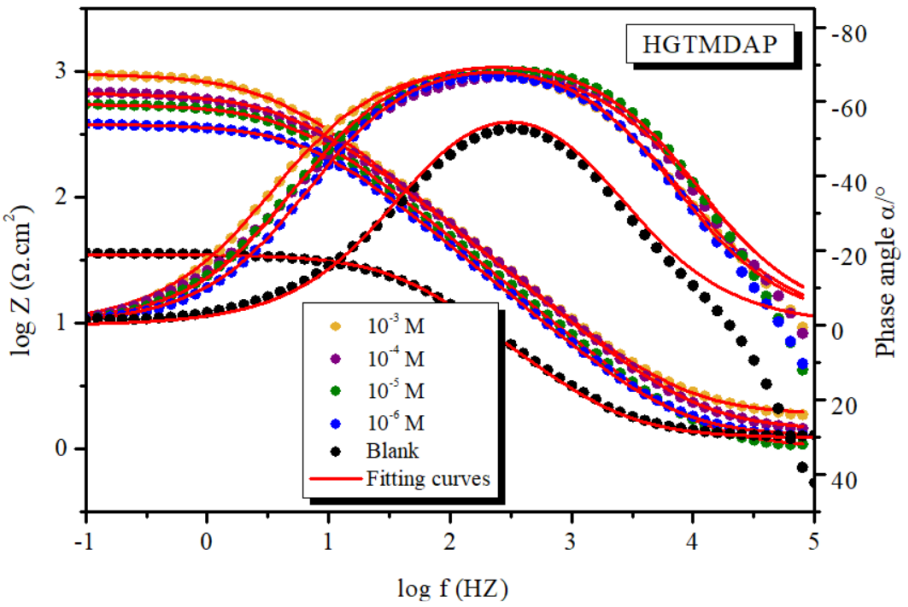

Figure 6: Bode diagram for blank and HGTMDAP at 298 K.

Table 4: EIS parameters for blank and HGTMDAP at 298 K.

Compound	**Conc. (M)**	R_s **(Ω.cm²)**	R_{ct} **(Ω.cm²)**	Q **(μF.S^{n-1})**	n_{dl}	**θ**	η_{EIS} **(%)**
1M HCl	-	1.12	34.7	419	0.773	-	-
HGTMDAP	10^{-6}	1.25	380.7	96.96	0.823	0.908	90.8
	10^{-5}	1.02	547.9	84.89	0.821	0.936	93.6
	10^{-4}	1.39	670.9	77.47	0.802	0.948	94.8
	10^{-3}	1.85	957.3	73.59	0.804	0.963	96.3

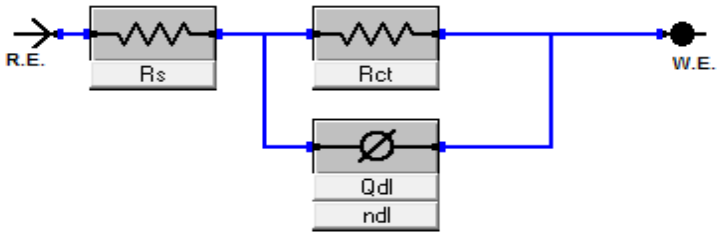

Figure 7: Equivalent electrical circuit of metal/ HGTMDAP/HCl.

3.3.1. Adsorption isotherm

The following main results were found related to adsorption isotherm and parameters:

The linear regression fit in Figure 8 confirms that the Langmuir isotherm model (Eq. 5) very well (R2 > 0.99) in the adsorption analysis.

$$\frac{C_{inh}}{\theta} = \frac{1}{K_{ads}} + C_{inh} \qquad (5)$$

The Langmuir isotherm suggests monolayer adsorption of the HGTMDAP on the homogeneous metal surface [41, 42]. The large positive value of the adsorption equilibrium constant (K_{ads} > 105 L/mol) implies strong interaction among HGTMDAP and metal surface. The calculated very negative Gibbs free energy of adsorption (ΔG_{ads} = -45.22 kJ/mol) (Eq. 6) confirms the spontaneity of the adsorption process and suggests it is predominantly physisorption through electrostatic interactions (**Table 5**).

$$K_{ads} = \frac{1}{55.5}\exp\left(\frac{-\Delta G^{\circ}_{ads}}{RT}\right) \qquad (6)$$

The thermodynamic parameter explains why HGTMDAP provides good inhibition even at high temperatures, as the adsorption process has a high affinity and is spontaneous.

In summary, the adsorption isotherm study provides useful mechanistic insights and quantitatively supports that HGTMDAP acts as an effective inhibitor through spontaneous physisorption.

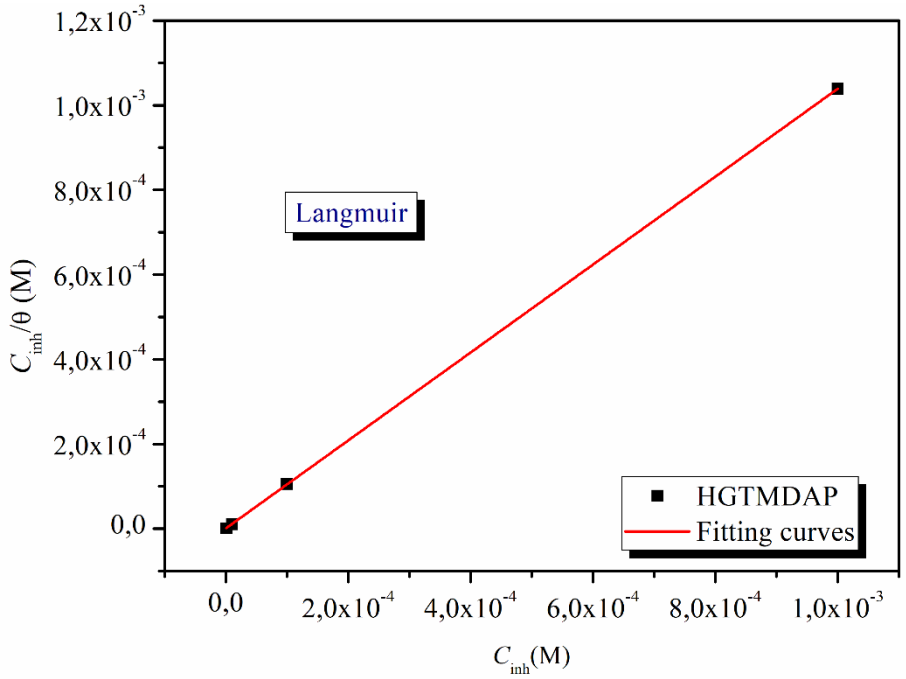

Figure 8: Langmuir adsorption isotherm for HGTMDAP at 298 K.

Table 5: Adsorption parameters of HGTMDAP at 298 K.

Inhibitor tested	**K_{ads} (L/mol)**	**R^2**	**ΔG_{ads} (kJ/mol)**
HGTMDAP	1525185.38	0.999	-45.22

3.4. Electrochemical frequency modulation

The key points from the EFM results are follows:

- ✓ EFM spectra show single activation energy distribution, reflecting the single corrosion mechanism [43, 44] (**Figure 9**).
- ✓ icorr and corrosion rate (CR) decrease with increasing inhibitor concentration, confirming better inhibition at higher C **(Table 6)**.
- ✓ Tafel slopes βa and βc are affected only slightly, indicating HGTMDAP acts as a mixed-type inhibitor.
- ✓ Protection values η rise with HGTMDAP values, achieving >95% efficiency at 10^{-3} M.
- ✓ CF values around 2 indicate slow reaction and presence of physical adsorption barrier.
- ✓ Excellent agreement between EFM and other techniques validates the chosen technique.
- ✓ Thermodynamic parameters from EFM are consistent with other results.

In summary, the obtained EFM details confirmed other techniques and provide microscopic confirmation that HGTMDAP functions via mixed inhibition mechanism by decreasing icorr through adsorption over a wide concentration range. The technique thus serves as a useful validation of corrosion inhibition process.

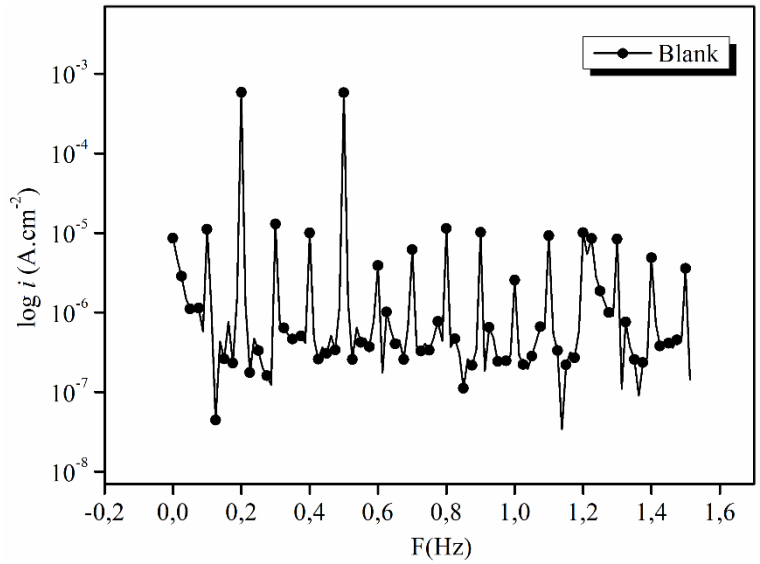
Blank
log i (A.cm-2)
F(Hz)

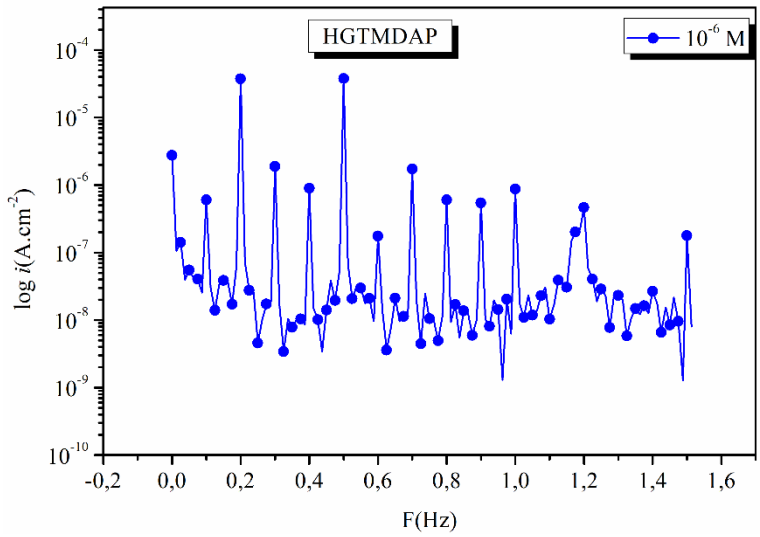
HGTMDAP
10-6 M
log i(A.cm-2)
F(Hz)

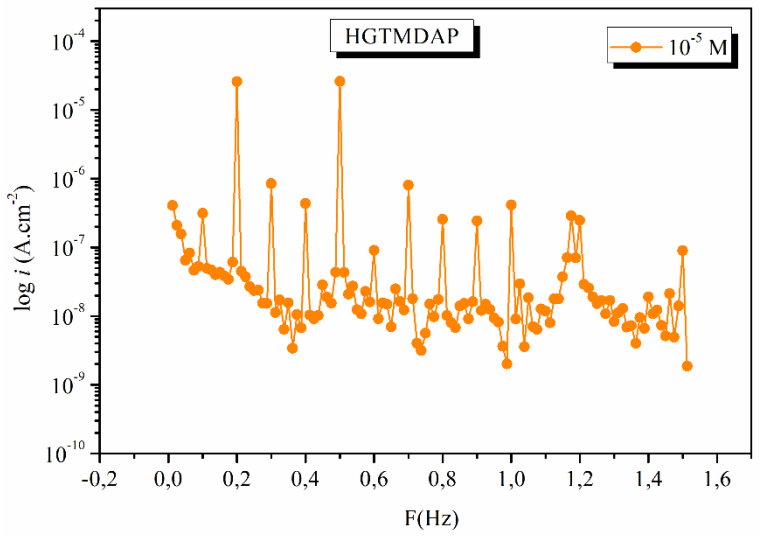
HGTMDAP
10-5 M
log i (A.cm-2)
F(Hz)

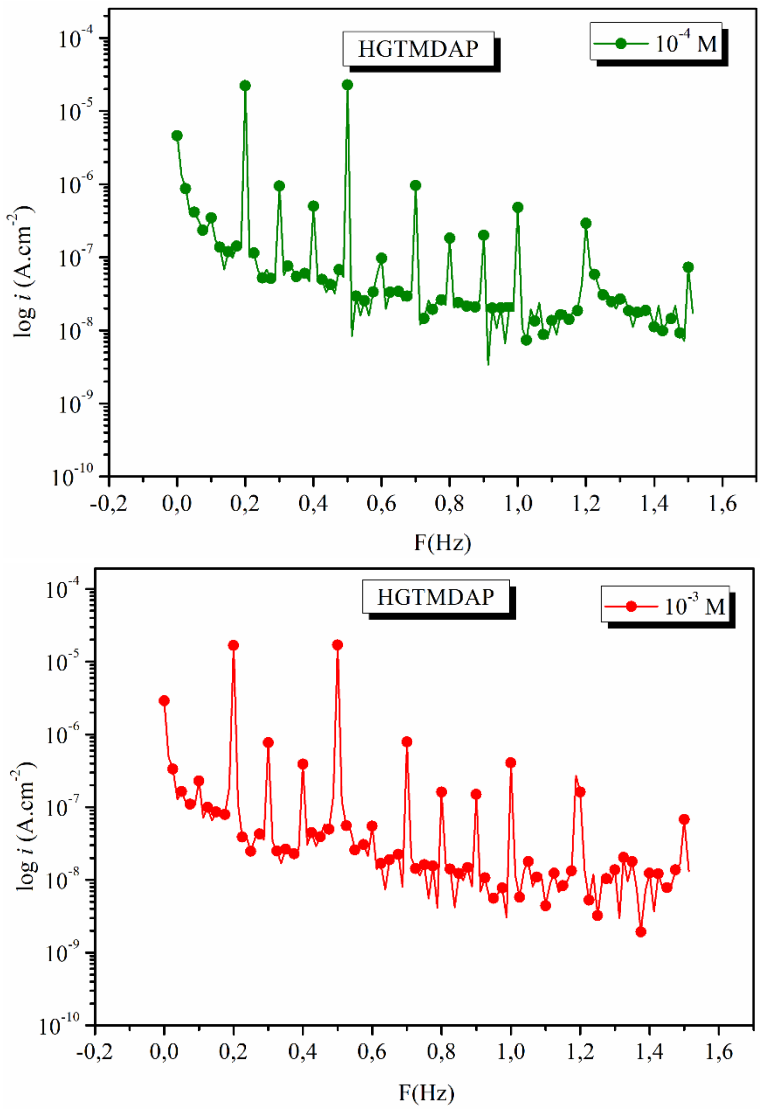

Figure 9: EFM spectra for blank and HGTMDAP at 228 K.

Table 6: Electrochemical kinetic parameters for blank and HGTMDAP at 228 K.

Compound	C (M)	%η	CF-3	CF-2	CR ($mm.y^{-1}$)	β_c, ($mVdec^{-1}$)	β_a ($mVdec^{-1}$)	i_{corr} ($\mu A\ cm^{-2}$)
1.0 M HCl	Blank	------	2.86	1.52	344.9	177	162	755
HGTMDAP	10^{-6}	92.49	3.1	2.03	25.90	114.4	85.57	56.68
	10^{-5}	93.8	2.9	1.9	21..18	131.1	104.4	46.36
	10^{-4}	94.9	3.0	1.9	17.57	130.1	97.32	38.45
	10^{-3}	95.9	2.86	1.95	13.9	141	100.7	30.42

3.5. Surface analysis (SEM/EDS)

SEM and EDS were employed to research the surface morphology and elemental composition of the metal after immersion in test solutions [45, 46]. This was done to complement the electrochemical findings. After immersion in 1.0 M HCl (Figure 10a), the SEM image revealed extensive surface corrosion characterized by non-uniform pits and cracks. The EDS spectrum showed prominent peaks for oxygen and chlorine, confirming the corrosive

nature of the test environment. In contrast, the steel surface immersed in 1.0 M HCl containing 10^{-3} M HGTMDAP inhibitor (Figure 10b) appeared smoother with fewer defects. The EDS analysis correspondingly detected weaker corrosion product peaks (oxygen, iron) along with new peaks for phosphorus and nitrogen from the inhibitor molecules. This suggests the formation of a protective layer on the steel by adsorption of the organic inhibitor compounds. The layer effectively slowed the corrosion process in acidic solution, corroborating the mechanism observed electrochemically. Thus, SEM/EDS complemented the electrochemical results by directly visualizing the difference in steel surface morphology and composition with and without inhibition. SEM was used to examine the surface morphology of the steel to complement and confirm the results of the electrochemical study. Next, the elemental chemical composition was determined using EDX analysis.

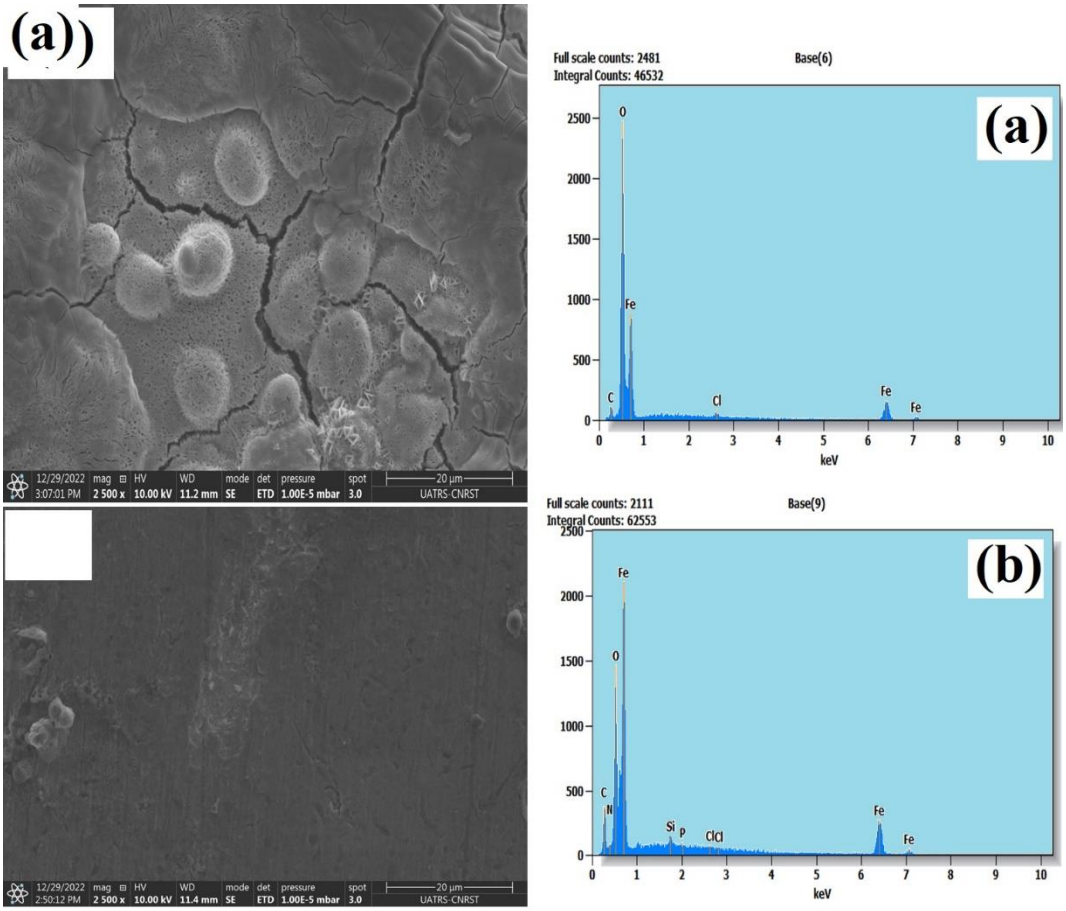

Figure 10: Scanning surface of metal electrode in 1.0 M HCl solution in the absence (a) and presence of 10^{-3} M HGTMDAP (b) SEM image and EDS spectrum.

3.6.Theoretical analysis

3.6.1. DFT results

The HGTMDAP inhibitor in neutral and protonated forms were utilised to do the DFT analysis [47-50].

The HOMO, LUMO orbitals and ESP pictures of the HGTMDAP inhibitor in neutral and protonated forms are plotted graphically in Figure 11.

It is indicated in Figure 11, the HOMO and LUMO regions are mainly located around methylene dianiline regions of both forms (HGTMDAP and HGTMDAP-H^+ forms).

The electrophilic and nucleophilic attack regions of HGTMDAP were illustrated in the ESP map [51, 52]. The nucleophilic (red) regions are positioned around O, N and P atoms, suggesting that these regions are covalent bonding centres. The corrosion inhibition was promoted by the nucleophilic (red) regions [53, 54].

The corrosion protection ability of this compound can also be evaluated by quantum chemical parameters given in Figure 11 and Table 7.

E_{HOMO} (HGTMDAP-H^+) < E_{HOMO} (HGTMDAP). This is because the higher the occupied high-orbit energy (E_{HOMO}), the greater the electron-donating capacity [55]. However, the lower the unoccupied orbital base energy, the higher the ability to accept electrons [56]. The energy gap (ΔE_{gap}) is considered an important factor in describing the statistical activity of the molecule, where the low value of ΔE_{gap} indicates the ease of electron transfer from the HOMO molecular orbital to the LUMO molecular orbital, and this translates into good inhibitory efficiency [57]. Consequently, neutral form (HGTMDAP) can be said to be more effective than protonated form.

- ✓ HOMO and LUMO regions are mainly localized around the methylene dianiline moiety for both neutral and protonated HGTMDAP forms.
- ✓ Neutral form shows wider nucleophilic regions (red color) around O, N and P atoms, indicating these are preferred coordination sites to metal surface.
- ✓ Higher EHOMO value for neutral form signifies greater electron donating ability to accept electrons from metal d-orbitals.
- ✓ Lower energy gap (ΔE_{gap}) for neutral form suggests easier electron transfer within the molecule and better inhibition.
- ✓ Calculated parameters like electron affinity, hardness, chemical potential etc. are in line with neutral form acting as a better chelating agent.
- ✓ Positive ΔN values \< 3.6 electron transfer suggests electron donation from both forms to steel surface favors inhibition.
- ✓ More negative $\Delta E_{back\text{-}donation}$ for protonated form indicates its lower electron back-donation ability.

Overall, the DFT study provides a microscopic understanding of inhibition mechanism at molecular level, corroborating better performance of neutral HGTMDAP form due to enhanced molecular interactions with steel surface through electron donation and back-donation according to polarization and charging effects. This lends theoretical support for experimental observations [58, 59].

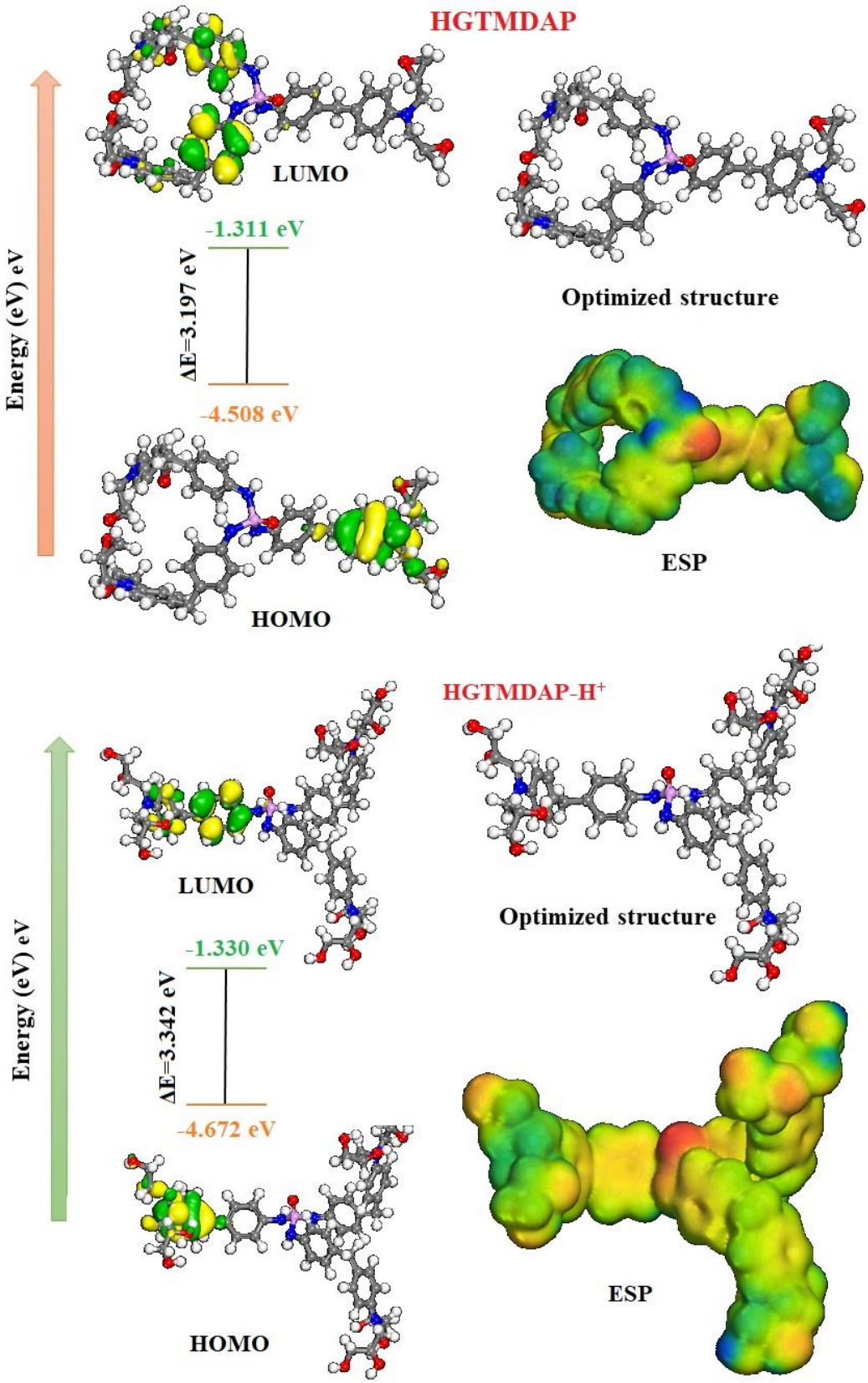

Figure 11: MD results of HGTMDAP and HGTMDAP-H^+.

Table 7: Reactivities for HGTMDAP and HGTMDAP-H^+.

Theoretical parameters	HGTMDAP	HGTMDAP -H^+
I (eV)	4.508	4.672
A (eV)	1.311	1.330

χ (eV)	2.909	3.001
η (eV)	1.598	1.671
σ (eV^{-1})	0.625	0.598
ΔN	0.598	0.544
$\Delta E_{back\text{-}donation}$	-0.399	-0.598

3.6.2. MC and MD simulations

To study and understand the interactions between inhibitor molecules and the metal surface, MC and MD simulations are frequently used (**Figures 12, 13 and 14**). The interactions between the HGTMDAP and HGTMDAP-H^+ inhibitor molecules and the metal surface were examined using MC and MD simulations. Strong connections between the inhibitor molecules and iron atoms through electron sharing were indicated by the simulations, which showed the molecules adsorbing almost parallel to the Fe(110) surface. Electron sharing from nitrogen, oxygen, and phosphorus atoms, as well as conjugated double bonds in the inhibitors with iron, facilitate chemical interactions. Physical adsorption is also facilitated by van der Waals forces. Adsorption energy (E_{ads}) calculations showed HGTMDAP-H^+ has stronger binding (-331.75 kcal/mol) than HGTMDAP (-327.35 kcal/mol), indicating inhibitory potency order. Radial distribution function (RDF) analysis calculated metal-nitrogen, oxygen and phosphorus bond lengths to identify adsorptive interactions. Bond lengths between 1-3.5 Å indicate chemisorption while >3.5 Å shows physisorption. Strong contact between inhibitors and iron substrate is confirmed by inhibitor atoms in RDF plots being close to the metal surface. The inhibitor molecules form Langmuir-type monolayer adsorption on the Fe surface, as indicated by their near-parallel orientation. This highest level of surface covering best prevents rusting. Chemisorption is the process by which strong chemical bonds form between the inhibitor and the metal surface by sharing electrons from nitrogen, oxygen, phosphorus, and conjugated bonds. This provides very strong inhibition. Van der Waals forces contribute to physisorption, a weaker physical interaction that still inhibits corrosion to some degree via blockage of surface area. More negative adsorption energies correspond to stronger binding of the inhibitor to the surface. The lower energy of HGTMDAP-H^+ suggests it forms stronger chemical bonds and will inhibit corrosion more effectively [60-63].

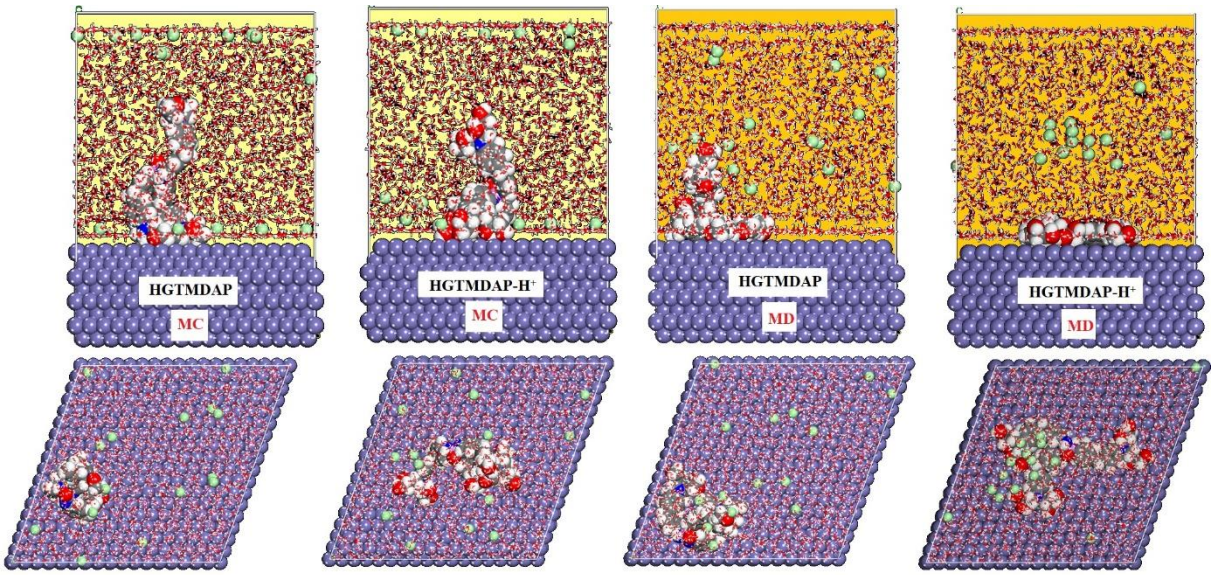

Figure 12: MC and MD simulation results for HGTMDAP and HGTMDAP-H^+ forms.

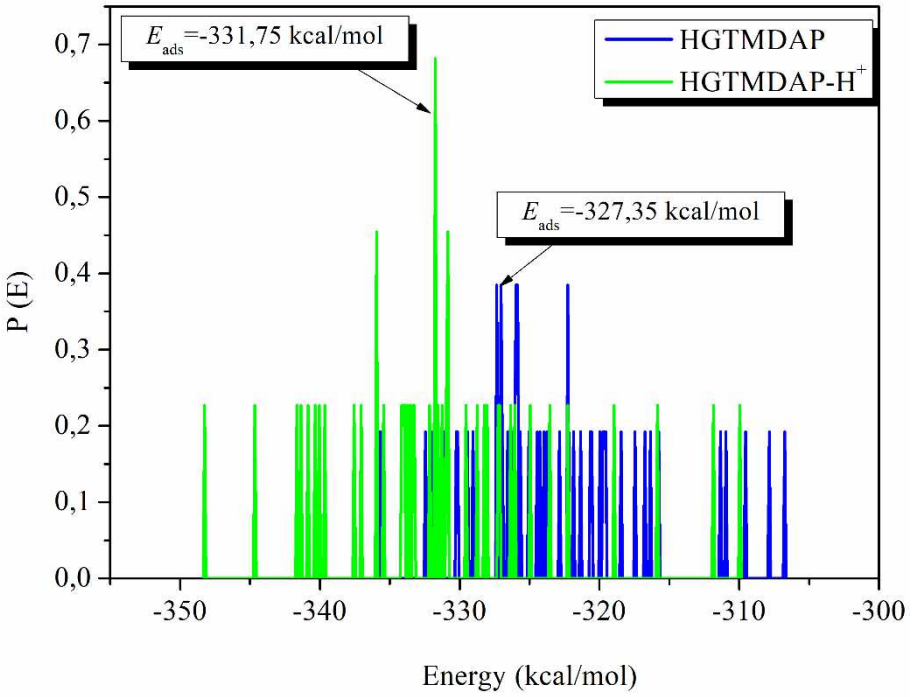

Figure 13: Distribution of the E_{ads} of HGTMDAP and HGTMDAP-H^+ forms on the Fe(110) surface.

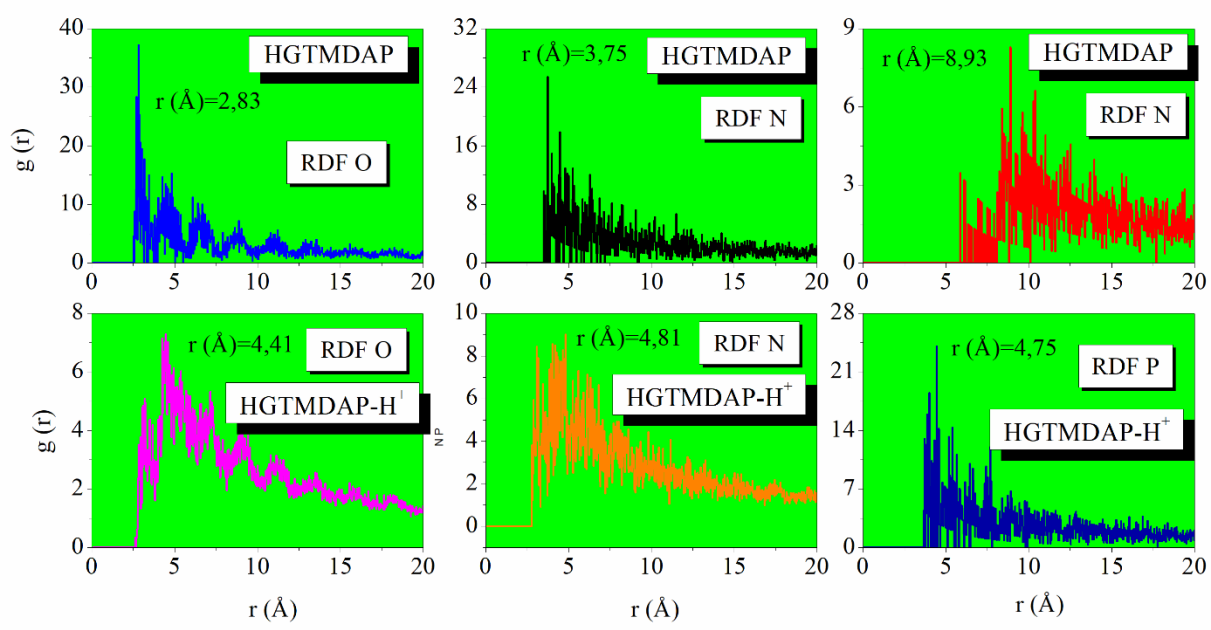

Figure 14: RDF O, N and P atoms of the HGTMDAP and HGTMDAP-H^+ forms.

4. Conclusion

The basic conclusions are:

- A new hexafunctional phosphorus epoxy resin (HGTMDAP) was successfully synthesized. Its structure was confirmed using FTIR and NMR techniques.
- Electrochemical techniques (EIS, PDP) showed that HGTMDAP acts as an effective mixed-type inhibitor for corrosion of carbon steel in 1 M HCl.
- Protection value rose with rising inhibitor concentration, reaching a maximum of 96.9% at 10^{-3} M based on PDP.
- EIS revealed a protection value of 96.3% for 10-3 M HGTMDAP, in agreement with PDP results.
- Thermodynamic parameters (Ea, ΔGads) and Langmuir isotherm confirmed monolayer adsorption of HGTMDAP on the steel surface.
- SEM/EDX showed HGTMDAP forms a defender layer on steel, inhibiting corrosion by separating steel from the corrosive electrolyte.
- Results from experimental and theoretical (DFT) techniques were in good agreement regarding the inhibition mechanism of HGTMDAP.

In summary, the new epoxy resin HGTMDAP showed high efficiency as a mixed-type protective agent for carbon steel in acid solution.

Funding

The authors received no direct funding for this research article.

Data Availability

All data generated or analyzed during this study are included in this published article.

Declarations

Conflict of interest

On behalf of all authors, the corresponding author

states that there is no conflict of interest.

References

[1] R. Hsissou *et al.*, "Novel derivative epoxy resin TGETET as a corrosion inhibition of E24 carbon steel in 1.0 M HCl solution. Experimental and computational (DFT and MD simulations) methods," *Journal of Molecular Liquids,* vol. 284, pp. 182-192, 2019.

[2] R. Hsissou *et al.*, "Development and potential performance of prepolymer in corrosion inhibition for carbon steel in 1.0 M HCl: outlooks from experimental and computational investigations," *Journal of colloid and interface science,* vol. 574, pp. 43-60, 2020.

[3] R. Hsissou *et al.*, "Trifunctional epoxy polymer as corrosion inhibition material for carbon steel in 1.0 M HCl: MD simulations, DFT and complexation computations," *Inorganic Chemistry Communications,* vol. 115, p. 107858, 2020.

[4] M. Rbaa *et al.*, "New Epoxy sugar based glucose derivatives as eco friendly protective agent s for the carbon steel in 1.0 M HCl: Experimental and theoretical investigations," *Journal of Alloys and Compounds,* vol. 833, p. 154949, 2020.

[5] O. Dagdag *et al.*, "Fabrication of polymer based epoxy resin as effective anti-corrosive coating for steel: Computational modeling reinforced experimental studies," *Surfaces and Interfaces,* vol. 18, p. 100454, 2020.

[6] O. Dagdag *et al.*, "Epoxy pre-polymers as new and effective materials for corrosion inhibition of carbon steel in acidic medium: Computational and experimental studies," *Scientific reports,* vol. 9, no. 1, pp. 1-14, 2019.

[7] O. Dagdag *et al.*, "Highly functionalized epoxy macromolecule as an anti-corrosive material for carbon steel: Computational (DFT, MDS), surface (SEM-EDS) and electrochemical (OCP, PDP, EIS) studies," *Journal of Molecular Liquids,* vol. 302, p. 112535, 2020.

[8] R. Hsissou, M. Berradi, M. El Bouchti, A. El Bachiri, and A. El Harfi, "Synthesis characterization rheological and morphological study of a new epoxy resin pentaglycidyl ether pentaphenoxy of phosphorus and their composite (PGEPPP/MDA/PN)," *Polymer Bulletin,* vol. 76, pp. 4859-4878, 2019.

[9] K. Ismaily Alaoui *et al.*, "Experimental and quantum chemical studies on corrosion protection ability of pyrazolic derivatives for mild steel in hydrochloric acid medium, correlation between electronic structure and inhibition efficiency," *Journal of Chemical and Pharmaceutical Research,* vol. 6, no. 7, pp. 63-81, 2014.

[10] R. Hsissou, B. Benzidia, N. Hajjaji, and A. Elharfi, "Elaboration and electrochemical studies of the coating behavior of a new nanofunctional epoxy polymer on E24 steel in 3.5% NaCl," *Portugaliae Electrochimica Acta,* vol. 36, no. 4, pp. 259-270, 2018.

[11] M. A. Amin and M. M. Ibrahim, "Corrosion and corrosion control of mild steel in concentrated H2SO4 solutions by a newly synthesized glycine derivative," *Corrosion Science,* vol. 53, no. 3, pp. 873-885, 2011.

[12] R. Hsissou, A. Bekhta, A. Elharfi, B. Benzidia, and N. Hajjaji, "Theoretical and electrochemical studies of the coating behavior of a new epoxy polymer: hexaglycidyl ethylene of methylene dianiline (HGEMDA) on E24 steel in 3.5% NaCl," *Portugaliae Electrochimica Acta,* vol. 36, no. 2, pp. 101-117, 2018.

[13] O. Dagdag *et al.*, "Polymeric-based epoxy cured with a polyaminoamide as an anticorrosive coating for aluminum 2024-T3 surface: experimental studies supported by computational modeling," *Journal of Bio-and Tribo-Corrosion,* vol. 5, pp. 1-13, 2019.

[14] R. A. Yukna *et al.*, "Multi-center clinical evaluation of combination anorganic bovine-derived hydroxyapatite matrix (ABM)/cell binding peptide (P-15) as a bone replacement graft material in human periodontal osseous defects. 6-month results," *Journal of periodontology,* vol. 69, no. 6, pp. 655-663, 1998.

[15] J. Andzelm, R. King-Smith, and G. Fitzgerald, "Geometry optimization of solids using delocalized internal coordinates," *Chemical physics letters,* vol. 335, no. 3-4, pp. 321-326, 2001.

[16] A. Berisha, "Interactions between the aryldiazonium cations and graphene oxide: A DFT study," *Journal of Chemistry,* vol. 2019, 2019.

[17] R. Peverati and D. G. Truhlar, "Performance of the M11 and M11-L density functionals for calculations of electronic excitation energies by adiabatic time-dependent density functional theory," *Physical Chemistry Chemical Physics,* vol. 14, no. 32, pp. 11363-11370, 2012.

[18] L. Goerigk and S. Grimme, "A thorough benchmark of density functional methods for general main group thermochemistry, kinetics, and noncovalent interactions," *Physical Chemistry Chemical Physics,* vol. 13, no. 14, pp. 6670-6688, 2011.

[19] Y. Inada and H. Orita, "Efficiency of numerical basis sets for predicting the binding energies of hydrogen bonded complexes: evidence of small basis set superposition error compared to Gaussian basis sets," *Journal of computational chemistry,* vol. 29, no. 2, pp. 225-232, 2008.

[20] O. Dagdag *et al.*, "DGEBA-polyaminoamide as effective anti-corrosive material for 15CDV6 steel in NaCl medium: Computational and experimental studies," *Journal of Applied Polymer Science,* vol. 137, no. 8, p. 48402, 2020.

[21] O. Dagdag *et al.*, "Polymeric-based epoxy cured with a polyaminoamide as an anticorrosive coating for aluminum 2024-T3 surface: experimental studies supported by computational modeling," *Journal of Bio-and Tribo-Corrosion,* vol. 5, no. 3, pp. 1-13, 2019.

[22] M. El Faydy *et al.*, "An experimental-coupled empirical investigation on the protective agent y action of 7-alkyl-8-Hydroxyquinolines on C35E steel in HCl electrolyte," *Journal of Molecular Liquids,* vol. 317, p. 113973, 2020.

[23] O. Dagdag *et al.*, "Epoxy resins and their zinc composites as novel anti-corrosive materials for copper in 3% sodium chloride solution: Experimental and computational studies," *Journal of Molecular Liquids,* vol. 315, p. 113757, 2020.

[24] Y. Karzazi, M. Belghiti, F. El-Hajjaji, and B. Hammouti, "Density functional theory modeling and monte carlo simulation assessment of N-substituted quinoxaline derivatives as mild steel protective agent s in acidic medium," *J Mater Environ Sci,* vol. 7, no. 10, pp. 3916-3929, 2016.

[25] S. K. Saha *et al.*, "Corrosion control of chrome steel ball in nitric acid medium using schiff base ligand and corresponding metal complexes: a combined experimental and theoretical study," *Can Chem Trans,* vol. 2, no. 4, pp. 381-402, 2014.

[26] L. Hu, S. Zhang, W. Li, and B. Hou, "Electrochemical and thermodynamic investigation of diniconazole and triadimefon as protective agent s for copper in synthetic seawater," *Corrosion Science,* vol. 52, no. 9, pp. 2891-2896, 2010.

[27] W. Li, L. Hu, S. Zhang, and B. Hou, "Effects of two fungicides on the corrosion resistance of copper in 3.5% NaCl solution under various conditions," *Corrosion Science,* vol. 53, no. 2, pp. 735-745, 2011.

[28] R. Hsissou, B. Benzidia, N. Hajjaji, and A. Elharfi, "Elaboration, electrochemical investigation and morphological study of the coating behavior of a new polymeric polyepoxide architecture: crosslinked and hybrid decaglycidyl of phosphorus pentamethylene dianiline on E24 carbon steel in 3.5% NaCl," *Portugaliae Electrochimica Acta,* vol. 37, no. 3, pp. 179-191, 2019.

[29] M. A. Amin and K. Khaled, "Copper corrosion inhibition in O2-saturated H2SO4 solutions," *Corrosion Science,* vol. 52, no. 4, pp. 1194-1204, 2010.

[30] P. Reena Kumari and D. Kumari, "Experimental and theoretical evaluation of rutin as eco-friendly protective agent for aluminum 6063 alloy in acidic medium," *Journal of Failure Analysis and Prevention,* vol. 18, no. 4, pp. 856-867, 2018.

[31] D. Zinad *et al.*, "A new synthesized coumarin-derived Schiff base as a protective agent of mild steel surface in HCl medium: gravimetric and DFT studies," *International Journal of Corrosion and Scale Inhibition,* vol. 9, no. 1, pp. 228-243, 2020.

[32] R. Murthy, P. Gupta, and C. Sundaresan, "Theoretical and electrochemical evaluation of 2-thioureidobenzheteroazoles as potent protective agent s for mild steel in 2 M HCl solution," *Journal of Molecular Liquids,* vol. 319, p. 114081, 2020.

[33] M. Ouakki *et al.*, "Investigation of imidazole derivatives as protective agent s for mild steel in sulfuric acidic environment: experimental and theoretical studies," *Ionics,* vol. 26, no. 10, pp. 5251-5272, 2020.

[34] I. Maamoun, R. Eljamal, O. Falyouna, K. Bensaida, Y. Sugihara, and O. Eljamal, "Insights into kinetics, isotherms and thermodynamics of phosphorus sorption onto nanoscale zero-valent iron," *Journal of Molecular Liquids,* vol. 328, p. 115402, 2021.

[35] G. Zhang, X. Hou, B. Hou, and H. Liu, "Benzimidazole derivatives as novel inhibitors for the corrosion of mild steel in acidic solution: Experimental and theoretical studies," *Journal of Molecular Liquids,* vol. 278, pp. 413-427, 2019.

[36] E. Ituen, A. James, and O. Akaranta, "Fluvoxamine-based protective agent s for J55 steel in aggressive oil and gas well treatment fluids," *Egyptian journal of petroleum,* vol. 26, no. 3, pp. 745-756, 2017.

[37] G. Fekkar *et al.*, "Eco-friendly Chamaerops humilis L. fruit extract protective agent for mild steel in 1 M HCl," *International Journal of Corrosion and Scale Inhibition,* vol. 9, no. 2, pp. 446-459, 2020.

[38] N. Iroha and L. Nnanna, "Tranexamic acid as novel protective agent for X60 steel in oil well acidizing fluids: surface morphology, gravimetric and electrochemical studies," *Progress in Color, Colorants and Coatings,* vol. 14, no. 1, pp. 1-11, 2021.

[39] D. Douche *et al.*, "Anti-corrosion performance of 8-hydroxyquinoline derivatives for mild steel in acidic medium: Gravimetric, electrochemical, DFT and molecular dynamics simulation investigations," *Journal of molecular liquids,* vol. 308, p. 113042, 2020.

[40] S. H. M. Jessima, S. Subhashini, and J. Arulraj, "Sunova spirulina powder as an effective environmentally friendly protective agent for mild steel in acid medium," *Journal of Bio-and Tribo-Corrosion,* vol. 6, pp. 1-13, 2020.

[41] F. El-Hajjaji *et al.*, "Time and temperature elucidation on steel corrosion inhibition by 3-methyl-1-prop-2-ynylquinoxalin-2 (1H)-one in molar hydrochloric acid: part 2," *J. Mater. Environ. Sci,* vol. 5, no. 1, p. 263, 2014.

[42] K. Adardour *et al.*, "Study of the influence of new quinoxaline derivatives on corrosion inhibition of mild steel in hydrochloric acidic medium," *J Mater Environ Sci,* vol. 1, pp. 129-138, 2010.

[43] R. Bosch, J. Hubrecht, W. Bogaerts, and B. Syrett, "Electrochemical frequency modulation: a new electrochemical technique for online corrosion monitoring," *Corrosion,* vol. 57, no. 1, pp. 60-70, 2001.

[44] S. Abdel-Rehim, K. Khaled, and N. Abd-Elshafi, "Electrochemical frequency modulation as a new technique for monitoring corrosion inhibition of iron in acid media by new thiourea derivative," *Electrochimica Acta,* vol. 51, no. 16, pp. 3269-3277, 2006.

[45] P. Zhao, Q. Liang, and Y. Li, "Electrochemical, SEM/EDS and quantum chemical study of phthalocyanines as protective agent s for mild steel in 1 mol/l HCl," *Applied Surface Science,* vol. 252, no. 5, pp. 1596-1607, 2005.

[46] M. Zouarhi *et al.*, "Evaluation of a new formulation derived from Aleurites moluccana seeds oil as a green protective agent for iron in acidic medium," *Anal. Bioanal. Electrochem,* vol. 11, pp. 1651-1668, 2019.

[47] M. Damej *et al.*, "New epoxy resin as a protective agent for the protection of carbon steel C38 in 1M HCl. experimental and theoretical studies (DFT, MC, and MD)," *Journal of Molecular Structure,* p. 132425, 2022.

[48] N. Bhardwaj, P. Sharma, A. Berisha, V. Mehmeti, O. Dagdag, and V. Kumar, "Monte Carlo simulation, molecular dynamic simulation, quantum chemical calculation and anti-corrosive behaviour of Citrus limetta pulp waste extract for stainless steel (SS-410) in acidic medium," *Materials Chemistry and Physics,* p. 126052, 2022.

[49] H. Jafari, E. Ameri, M. Rezaeivala, A. Berisha, and J. Halili, "Anti-corrosion behavior of two N2O4 Schiff-base ligands: Experimental and theoretical studies," *Journal of Physics and Chemistry of Solids,* vol. 164, p. 110645, 2022.

[50] B. O. Abdelwedoud *et al.*, "Inhibition effect of N-propargyl saccharin as protective agent of C38 steel in 1 M HCl, experimental and theoretical study," *Journal of Molecular Liquids,* vol. 354, p. 118784, 2022.

[51] O. Dagdag *et al.*, "Synthesis, physicochemical properties, theoretical and electrochemical studies of tetraglycidyl methylenedianiline," *Journal of Molecular Structure,* vol. 1265, p. 133508, 2022.

[52] W. Daoudi *et al.*, "Essential oil of Dysphania ambrosioides as a green protective agent for mild steel in HCl solution," *Journal of Molecular Liquids,* vol. 363, p. 119839, 2022.

[53] G. Bahlakeh, B. Ramezanzadeh, A. Dehghani, and M. Ramezanzadeh, "Novel cost-effective and high-performance green inhibitor based on aqueous Peganum harmala seed extract for mild steel corrosion in HCl solution: Detailed experimental and electronic/atomic level computational explorations," *Journal of Molecular Liquids,* vol. 283, pp. 174-195, 2019.

[54] I. Hermoso-Diaz, A. Foroozan, J. Flores-De los Rios, L. Landeros-Martinez, J. Porcayo-Calderon, and J. Gonzalez-Rodriguez, "Electrochemical and quantum chemical assessment of linoleic acid as a protective agent for carbon steel in sulfuric acid solution," *Journal of Molecular Structure,* vol. 1197, pp. 535-546, 2019.

[55] O. Dagdag *et al.*, "Epoxy prepolymer as a novel anti-corrosive material for carbon steel in acidic solution: electrochemical, surface and computational studies," *Materials Today Communications,* vol. 22, p. 100800, 2020.

[56] O. Dagdag *et al.*, "Synthesis of macromolecular aromatic epoxy resins as anticorrosive materials: computational modeling reinforced experimental studies," *ACS omega,* vol. 5, no. 7, pp. 3151-3164, 2020.

[57] O. Dagdag *et al.*, "Anticorrosive property of heterocyclic based epoxy resins on carbon steel corrosion in acidic medium: Electrochemical, surface morphology, DFT and Monte Carlo simulation studies," *Journal of Molecular Liquids,* vol. 287, p. 110977, 2019.

[58] N. Yilmaz, A. Fitoz, and K. C. Emregül, "A combined electrochemical and theoretical study into the effect of 2-((thiazole-2-ylimino) methyl) phenol as a protective agent for mild steel in a highly acidic environment," *Corrosion Science,* vol. 111, pp. 110-120, 2016.

[59] I. Lukovits, E. Kalman, and F. Zucchi, "Protective agent s—correlation between electronic structure and efficiency," *Corrosion,* vol. 57, no. 1, pp. 3-8, 2001.

[60] R. Ganjoo *et al.*, "Experimental and theoretical study of Sodium Cocoyl Glycinate as protective agent for mild steel in hydrochloric acid medium," *Journal of Molecular Liquids,* vol. 364, p. 119988, 2022.

[61] W. Daoudi *et al.*, "New chlorophenyl-imidazole derivative as a novel protective agent in the gas and oil industry," *Journal of Physics and Chemistry of Solids,* vol. 179, p. 111409, 2023.

[62] W. Daoudi *et al.*, "Anti-corrosion coating formation by a biopolymeric extract of Artemisia herba-alba plant: Experimental and theoretical investigations," *Coatings,* vol. 13, no. 3, p. 611, 2023.

[63] N. Bhardwaj, P. Sharma, A. Berisha, V. Mehmeti, O. Dagdag, and V. Kumar, "Monte Carlo simulation, molecular dynamic simulation, quantum chemical calculation and anti-corrosive behaviour of Citrus limetta pulp waste extract for stainless steel (SS-410) in acidic medium," *Materials Chemistry and Physics,* vol. 284, p. 126052, 2022.

Supplementary Files

This is a list of supplementary files associated with this preprint. Click to download.

- SI7.docx